



Fiber Laser-Assisted Synthesis of MoS₂ Nanomaterials for Enhanced Anticancer and Antibacterial Activity

Layal A. Jasim^{1*}, Fatema H. Rajab¹ and Ahmad W. Alshaer²

¹Department of Laser and Optoelectronics Engineering, College of Engineering, Al-Nahrain University, Jadyria, Baghdad, Iraq, 1007

²School of Engineering, University of Central Lancashire, Preston, UK.

ARTICLE INFO

Article history:

Received January 26, 2025

Revised May 6, 2025

Accepted May 10, 2025

Available online June 1, 2025

Keywords:

Fiber laser

Nanomaterials

MoS₂-CS

MoS₂-PEG

Antibacterial

Anticancer

ABSTRACT

Molybdenum disulfide (MoS₂) is a promising nanomaterial with a wide range of applications. Its outstanding properties, good biocompatibility, and band gap characteristics allow it to be used in biosensing, electronics, optoelectronics, and biological and medical applications. Furthermore, Biopolymers, including chitosan and PEG, are regarded as the most promising materials in the medical domain. This work aims to synthesize MoS₂, MoS₂-CS, and MoS₂-PEG using laser ablation and study their morphological characteristics, antibacterial, and anticancer activities. Therefore, MoS₂ nanoparticles are generated using a Fiber laser in this work. Then, the MoS₂-Cs and MoS₂-PEG nanocomposites were prepared by adding previously prepared MoS₂ particles to the CS and PEG polymers. A comprehensive examination of the manufactured composites was performed using X-ray diffraction analysis (XRD), transmission electron microscopy (TEM), ultraviolet-visible spectroscopy (UV-Vis), energy Dispersive X-ray (EDX), Raman spectroscopy, and Fourier transform infrared spectroscopy (FTIR) to validate the quality and content of the newly prepared composites. Based on the results, MoS₂NPs show a minimum average size of 20 nm generated using 3.2 J/m², 250 mm/s, 127 ns pulse duration, 30 Hz pulse repetition rate, and 3 minutes irradiation. Furthermore, the recorded average size of MoS₂-CS and MoS₂-PEG nanocomposite were 10.5 nm and 7.8 nm, respectively. The MoS₂-CS hybrid nanocomposite showed the highest antibacterial activity against E. coli bacteria, while MoS₂-CS and MoS₂-PEG showed the highest antibacterial activity against S. aureus bacteria compared to pure MoS₂ NPs. The anticancer analysis demonstrated that the MoS₂-CS nanocomposite presented the highest cytotoxic effect against the A549 cell compared to MoS₂ and MoS₂-PEG.

1. Introduction

In recent years, there has been a growing interest in 2D nanomaterials due to advancements in nanotechnology [1]. Nowadays, there has been significant progress in the development of MoS₂ nanomaterials for applications in energy storage [2], electronics [3], and catalysis [4]. The use of MoS₂ nanoparticles in biomedicine has emerged as a new and highly discussed subject in recent

years. These materials exhibit greater sensitivity and may be used as excellent nano-probes for cancer therapy [5-7] and antibacterial agents [8]. MoS₂ nanomaterials are used in constructing various biosensors due to their advantageous characteristics, including a high surface-to-volume ratio and exceptional stability. Recently, they have been regarded as a potential platform for detecting biomolecules [1,9].

* Corresponding author.

E-mail address: st.layal.abdulkareem.msc@ced.nahrainuniv.edu.iq

DOI: [10.24237/djes.2024.18205](https://doi.org/10.24237/djes.2024.18205)

This work is licensed under a [Creative Commons Attribution 4.0 International License](https://creativecommons.org/licenses/by/4.0/).



There are many ways to prepare MoS₂ nanomaterials, including various top-down and bottom-up approaches, such as Chemical Vapour Deposition (CVD) [10] electrochemical exfoliation, laser ablation, plasma etching, and mechanical cleavage [11-15]. Despite the advancements made thus far, most methodologies remain time-consuming and highly sensitive, and environmental conditions limit their use in small-scale applications [16]. To satisfy the need for green synthesis in nanotechnology, it is essential to provide alternative methods for simple, rapid, and large-scale production. This makes the proposed pulse laser ablation method suitable for preparing MoS₂ nanoparticles and MoS₂-based hybrid composite materials. Liquid-based pulsed laser ablation has become popular due to the excellent properties of the nanomaterials produced. Production methods affect the size and shape of nanomaterials, which determine their properties [17]. Pulsed Laser Ablation in Liquid Phase (PLAL) involves focusing a laser beam onto a material's surface. The intense radiation causes a series of effects—heating, melting, evaporation, and eventually plasma formation. As the laser interacts with the material, it excites atomic vibrations, generating heat and weakening molecular bonds. Continued exposure leads to melting and evaporation, and with sufficient energy, the vapor ionizes to form plasma. A liquid may then absorb and rapidly cool the plasma to create the desired nanomaterials [18]. This approach has multiple benefits, including its simplicity, cost-effectiveness, efficiency, and lack of chemical components. It also generates nanoparticles free from contamination and does not result in environmental pollution [19].

Several works have focused on generating MoS₂ nanomaterials using laser technology. Le Zhou et al. [20] fabricated spherical and onion-like structures of MoS₂ NPs with 10-100nm in diameter using 1064nm, 10ns laser ablation in water. Makoto Kanazawa et al. [21] synthesized MoS₂ nanoparticles using 10ns, 532nm Nd: YAG laser for 120 minutes on samples immersed in various solvents (ethanol, methanol, and NMP of 40 ml), and they found that the size and morphology of MoS₂ NPs

depended on the nature of the solvent used during laser ablation. Samira Moniri et al. [22], [23] prepared MoS₂ NPs by nanosecond laser ablation in ethylene glycol using a Q-switched Nd: YAG laser at different wavelengths (1064 and 532 nm). They reported that the mean particle size dropped from 22 to 13 nm when the laser wavelength was raised because of a photo fragmentation phenomenon. Fan Ye et al. [24] employed femtosecond laser irradiation (800 nm wavelength, 35 fs pulse duration, 1 kHz repetition rate) to produce MoS₂ nanosheets with an average diameter of 30 nm. The synthesis involved dispersing MoS₂ powder in a mixed ethanol-water solution. They examined the effects of laser exposure duration and ethanol concentration on the oxidation behavior of the resulting nanomaterials and compared the outcomes with those from a traditional hydrothermal approach. The study demonstrated that femtosecond lasers effectively disrupted the chemical bonds in MoS₂. It was concluded that ethanol concentrations of 80% and 90% were optimal for generating plasmonic MoO_{3-x} after 30 minutes of irradiation, highlighting its potential application in photothermal cancer therapy.

ZUO Pei et al. [25] prepared MoS₂ core-shell NPs through an fs laser system with parameters of 20 μm scan spacing, 400 μm/s scan speed, 250 μJ pulse energy, and 1 h scan time. They irradiated the MoS₂ bulk target in different concentrations of sodium chloride solution and achieved a 28 nm average diameter of MoS₂ NPs. The MoS₂ core-shell NPs were used as a reducing agent, which could be used as SERS substrates for biological and chemical sensing. Recently, Zekun Wang et al. [26] fabricated MoS₂ electrodes using a combination of fs laser and hydrothermal synthesis.

It has been reported that Polyethylene Glyco (PEG) has high absorbance and biocompatibility, making it suitable for drug delivery systems and improving the solubility and stability of MoS₂ in biological environments [27], [28]. Indeed, chitosan is known for its biocompatibility and biodegradability, and it can be used in wound dressings, drug delivery, and tissue engineering applications when combined with MoS₂ [29]. Zhang et al. reported

that chitosan (CS) functionalized magnetic MoS₂ nanocomposite, infused with iron oxide NPs, showed considerable antibacterial efficacy resulting from the combined effects of magnetic field-assisted bacterial enrichment and near-infrared (NIR) induced thermal generation [30].

Liu and co-workers demonstrated that the PEG-MoS₂ composite could be a multi-functional drug carrier for integrating photothermal and chemotherapy into a single compound. Two-dimensional MoS₂-PEG nanomaterials show strong NIR absorbance, which makes them a promising candidate for photothermal therapy with anticancer effect [31].

To our knowledge, many published publications are focusing on the synthesis of MoS₂ nanomaterials using laser ablation in liquids. Furthermore, there is no published work focused on the generation of MoS₂ NPs using a fiber laser. Indeed, the generation of MoS₂-CS and MoS₂-PEG nanocomposites for biological applications using laser technology has not been

reported yet. Therefore, this work focuses on synthesizing MoS₂, MoS₂-CS, and MoS₂-PEG nanocomposites using fiber laser ablation in a water environment and studying their morphological characteristics and biomedical properties.

1. Materials and methods

1.1 Fiber laser generation of nanomaterials

Molybdenum disulfide (MoS₂) from Boyan Optical Co., Ltd, in the form of a disk with 99.9% purity and a diameter of 20mm with a 2mm thickness, was used as a target material to prepare MoS₂ nanoparticles. As shown in Figure 1, the MoS₂ target was placed at the bottom of a glass vessel containing 3 mL of deionized water. MoS₂ nanoparticles were synthesized by ablating a molybdenum disulfide plate with a 1064 nm pulsed fiber laser using line-by-line scanning and processing parameters listed in Table 1.

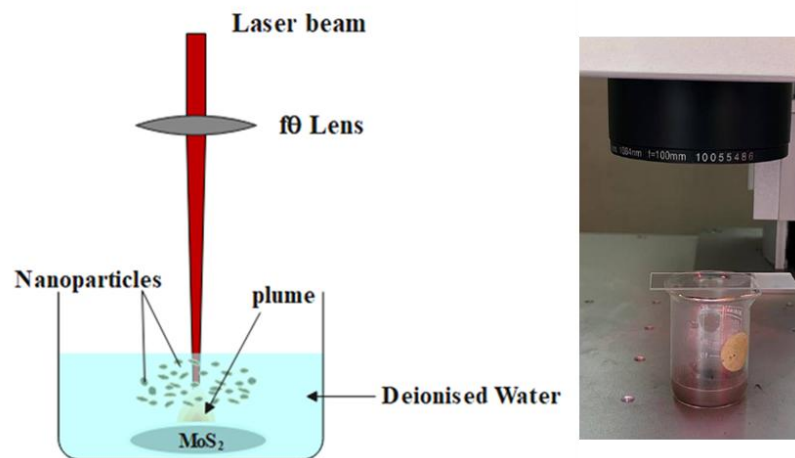


Figure 1. A schematic representation of laser ablation to MoS₂ in a solvent

Table 1: The laser processing parameters

Laser Parameters	Details
Fluence [J/m ²]	3.2
Scanning speed [mm/s]	250
Processing time [minutes]	3
Pulse repetition rate [kHz]	30
Focal length [mm]	100
Pulse duration [ns]	127
Spot size [μm]	100

After laser-generated pure MoS₂ NPs, the nanocomposites were produced using a green

sonochemistry method [32]. For MoS₂-PEG nanocomposite preparation, a solution of 3 mL

of MoS₂ nanoparticles was initially combined with 0.1g of PEG through vigorous stirring. The mixture was then stirred at room temperature, with a stirring speed of 700 rpm, for 30 min. Following the stirring step, sonication, which is a process that utilizes high-frequency sound waves to promote the dispersion and interaction of particles within a solution, was performed using an ultrasonic probe with a power output of 150 W for 10 minutes at a temperature ranging from 25 to 35 °C. This ultrasonic treatment enhanced the dispersion and interaction between the MoS₂ nanoparticles and the polymer solution. The same method was used to synthesize the MoS₂-CS, but before combining the MoS₂ with chitosan, the chitosan solution was prepared by dissolving 1 g of chitosan in 50 ml of 0.5% acetic acid.

1.2 Characterization of synthesized nanomaterials

The UV–visible absorption spectra of as-prepared MoS₂, MoS₂-CS, and MoS₂-PEG NPs were examined using a SHIMADZU UV-VIS (1900i/ Japan) spectrophotometer. Fourier transform infrared (FTIR) spectra were applied using a SHIMADZU IR Affinity (-1 plus / Japan) spectrometer from 400 to 4000 cm⁻¹. Transmission Electron Microscopy (TEM), a Zeiss-EM10C-100 KV, is used to determine the morphology and structure of the composite samples. X-ray diffraction is a method for examining materials' crystal structure and phase makeup; the Panalytical X-ray diffractometer (type PW1730) is outfitted with Cu K radiation ($\lambda=1.5406 \text{ \AA}$) at room temperature. The sample for the X-ray assay was prepared by dropping the solution on a glass substrate and then drying it in the air. The obtained samples' chemical composition was determined using an Energy Dispersive X-ray (EDX) inspect S50 (FEI company, the Netherlands). To disclose the chemical constituents, a few drops of colloidal solution were put into the glass slides to prepare the samples for analysis, after which the slides were allowed to air dry at ambient temperature. The analysis uses Raman (XploRA Plus, Jaban).

1.3 Antibacterial activity

Muller-Hinton (M-H) agar was created by dissolving 20 mL of the powder in 1 L of distilled water, followed by heating on a burner with continuous agitation. The M-H agar was then autoclaved for 15 minutes at 121°C for sterilization. After autoclaving, the agar was allowed to cool to 50°C before being poured into Petri dishes and left to solidify for approximately 15 minutes. Once solidified, the plates were inverted and stored at 4°C for further use. The antibacterial activity of the prepared samples (MoS₂, MoS₂+PEG, MoS₂+CS, PEG, CS) was evaluated against Gram-negative and Gram-positive bacterial strains using the agar well diffusion method. Approximately 20 mL of Muller-Hinton (MH) agar was aseptically poured into sterile Petri dishes. The bacterial species were obtained from stock cultures using a sterile inoculation loop. After inoculating the organisms, wells with a 6 mm diameter were created in the agar plates using a sterile tip. The plates, containing the samples (MoS₂, MoS₂+PEG, MoS₂+CS, PEG, CS) and the test bacteria, were incubated overnight at 37°C. The zones of inhibition were measured, and the average diameters were recorded. The data underwent statistical analysis with GraphPad Prism software. Results are presented as the mean \pm standard deviation from three separate trials. A statistically significant difference was defined as $p < 0.05$ [33].

1.4 Anticancer test

Lung adenocarcinoma A549 cell lines were maintained in RPMI-1640 (Capricorn, Germany) supplemented with 10% fetal bovine serum (Capricorn, Germany), 100 units/mL penicillin, and 100 $\mu\text{g/mL}$ streptomycin. Cells were passaged with Trypsin-EDTA (Capricorn, Germany), reseeded at 80% confluence biweekly, and incubated at 37 °C. To determine the cytotoxic effect of (MoS₂, MoS₂-PEG, and MoS₂-CS) nanocomposite materials, the MTT test was conducted on 96-well plates. Cell lines were inoculated at a density of 1×10^4 cells per well. A confluent monolayer was achieved after 24 hours, and A549 cells were treated with

(MoS₂, MoS₂-PEG, MoS₂-CS). Cell viability was assessed at 24, 48, and 72 hours post-treatment with MoS₂, MoS₂-PEG, and MoS₂-CS by replacing the medium, adding 100 μ L of a 2 mg/mL MTT solution, and incubating the cells for 2.5 hours at 37 °C. After the elimination of the MTT solution (Bio-World, USA), the crystals remaining in the wells were solubilized by the addition of 130 μ L of DMSO (Dimethyl Sulphoxide) (Santacruz Biotechnology, USA), followed by incubation at 37 °C for 15 minutes with agitation. Absorbance was quantified using a microplate reader at 492 nm; the assay was performed in triplicate. The cell growth inhibition rate (cytotoxicity percentage) was determined using the following equation[34].

$$\text{Inhibition rate} = (A - B)/(A * 100) \quad (1)$$

A represents the optical density of the control, whereas B denotes the optical density of the samples.

To observe the morphology of the cells using an inverted microscope, the cells were inoculated onto 24-well microtitration plates at a density of 1×10^5 cells mL⁻¹ and incubated for 24 hours at 37 °C. Then, cells were exposed to (MoS₂, MoS₂+PEG, MoS₂+CS) for 24hr. After exposure, the plates were treated with crystal violet dye and incubated at 37 °C for 10 to 15 minutes. The stain was meticulously rinsed with tap water until the color was eliminated. The cells were examined using an inverted microscope at 100 \times magnification, and photographs were recorded using a digital camera connected to the microscope [35]. The acquired data were statistically evaluated using an unpaired t-test utilizing GraphPad Prism 6. The data were expressed as the mean \pm standard deviation of triplicate measurements.

2. Results and discussion

UV-Vis absorption spectroscopy is also used for the quantitative analysis of produced nanocomposites. Figure 2 depicts the UV-Vis absorbance spectra of MoS₂, MoS₂-Chitosan (MoS₂-CS), and MoS₂-PEG composites. The lowest absorbance intensity of pristine MoS₂ in the studied wavelength region is indicative of the intrinsic semiconducting character of MoS₂.

The absorbance is notably improved with the addition of chitosan and PEG, with MoS₂-PEG resulting in the greatest intensity. The enhancement identifies that MoS₂ is better dispersed and stabilized in polymer matrices than PEG, exhibiting a stronger stabilizing effect over chitosan. In the UV region (200–400 nm), all samples show characteristic electronic transition of MoS₂, and peaks for the composites are shifted or smoothed, which indicates that there are interactions between MoS₂ and the polymers. This increase of absorbance around 253 nm is due to hydrogen bonding or electrostatic interactions between chitosan and MoS₂, allowing moderate stabilization and dispersion of the MoS₂ in this composite. Conversely, the large absorbance increase of MoS₂-PEG further emphasizes the role of PEG in enabling a more uniform coating around the MoS₂ layer, thereby diminishing aggregation and improving the optical properties. In the visible region (>400 nm), the absorbance decreases for all samples as it can be expected from the MoS₂-based materials. On the other hand, MoS₂-PEG exhibits greater absorbance, which probably results from enhanced light scattering or better homogeneity. These conclusions further establish that chitosan (or PEG) incorporation into MoS₂ systems serves as a successful modifier for their optical properties and that PEG provides a better stabilization. This renders MoS₂-PEG as a promising candidate for enhanced optical activity and stability in applications, such as bioimaging or photothermal therapy [36].

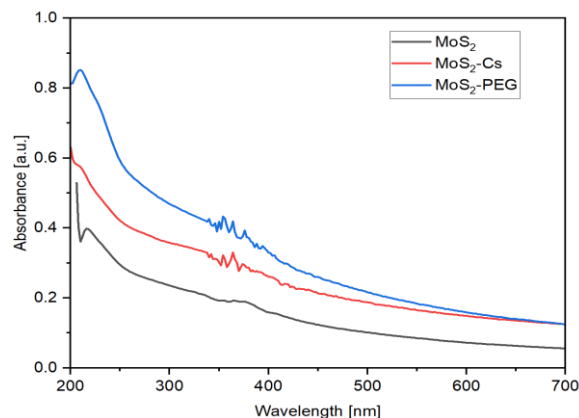


Figure 2. The UV-Vis absorption of as-prepared pure NPs and hybrid nanocomposites

The TEM micrographs of pristine MoS₂, MoS₂-Chitosan (MoS₂-CS), and MoS₂-PEG composites are shown in Figure 3. Well-defined nanosheets with certain degree of agglomeration can be observed in the images of pristine MoS₂ (Figure 3a) as per its characteristic layered structure. They observe the spherical particles that are likely due to the native morphology of MoS₂ or contaminants. These sheets seem thick and stacked, suggestive of minimal exfoliation and the naturally layered character of MoS₂. The size distribution of NPs ranges from 1.4 to 227.8 nm, with an average size of 20.2nm. The penetration of chitosan changes the morphology dramatically in the case of MoS₂-CS (Figure 3b). The images show partially exfoliated MoS₂ sheets with lower aggregation in comparison to pristine MoS₂. The increased performance is due to chitosan's ability to bond onto MoS₂ with hydrogen bonds or participating in electrostatic interactions and prevents the restacking of the nanosheets. Moreover, a thin, amorphous coating over the MoS₂ sheets indicates a homogeneous deposition of chitosan all over the MoS₂ surface.

The aggregation dropping further is visible for MoS₂-PEG (Figure 3c), suggesting well-dispersed nanosheets. The images suggest that PEG coats the MoS₂ sheets more uniformly, hinders restacking, and enhances exfoliation.

This uniform distribution could be attributed to PEG's hydrophilic property which enable effective interaction and stability of the MoS₂ nanosheets. The spherical nanoparticles embedded into the PEG matrix indicate the better stabilization of MoS₂ and dispersion of the MoS₂ in polymer. The size of NPs using CS and PEG record an average size of 10.5nm and 7.8nm, respectively. The TEM results clearly indicate that both chitosan and PEG considerably affect the morphology and dispersion of MoS₂. Although chitosan behaves as a partial exfoliator and hinders aggregation, it does not render as stable and well-dispersed matrix as PEG, since during the MoS₂ working, PEG keeps a homogenous structure and wraps the entire MoS₂ layers. The enhanced morphology also translates to better performance of the composites in specific applications [37].

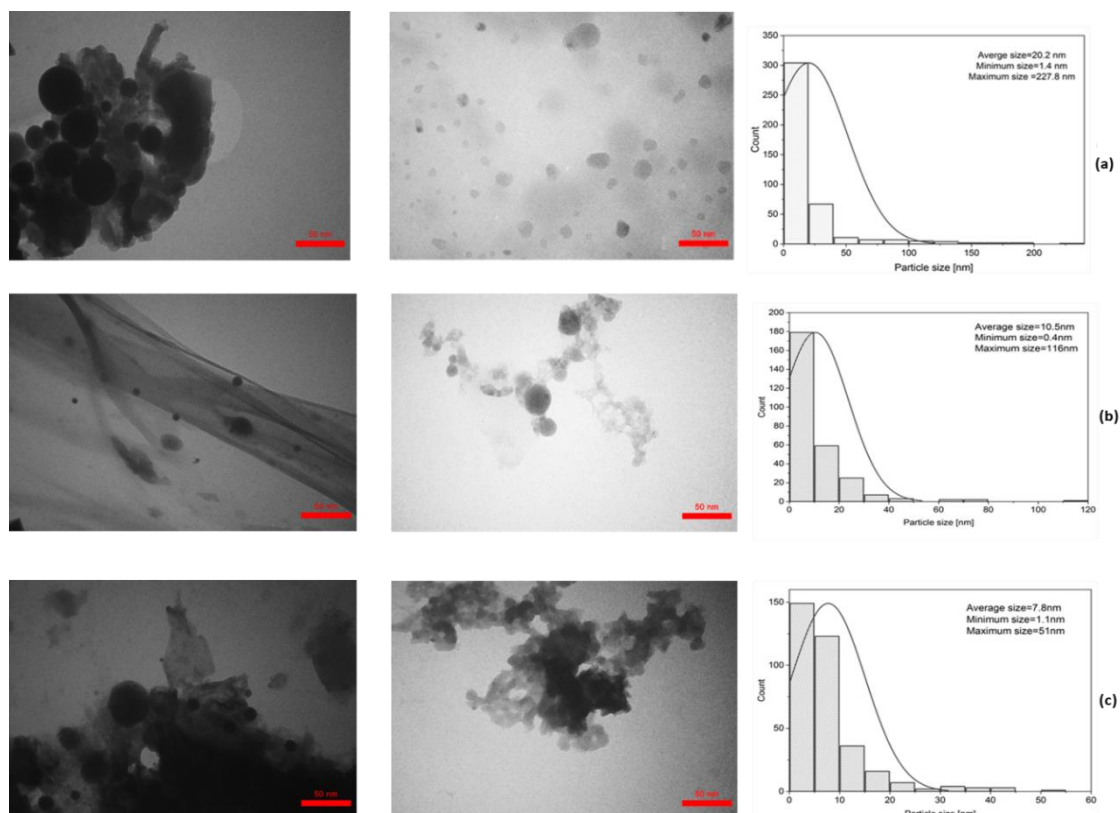


Figure 3. TEM images of (a) pure MoS₂, (b) MoS₂-CS, and (c) MoS₂-PEG

The EDX was performed to assess the elemental distribution of the synthesized nanomaterials. It can be observed that the elements Mo and S are uniformly distributed in the studied area (Figure 4a). The atomic percentage of Mo, S, and O is 31.97%, 52.85%, and 15.18%, respectively. The figure reveals the dominance of Mo and S, which are the primary components of MoS₂, and the oxygen might be

attributed to the water. The EDX spectrum of MoS₂-CS and MoS₂-PEG nanocomposites is shown in Figures 4b and c. It can be seen that the main components are C and O, which recorded atomic ratios of 75.25% (C) and 27.74% (O) in the case of MoS₂-PEG and 60.77% (C) and 32.63% (O) in the case of MoS₂-CS.

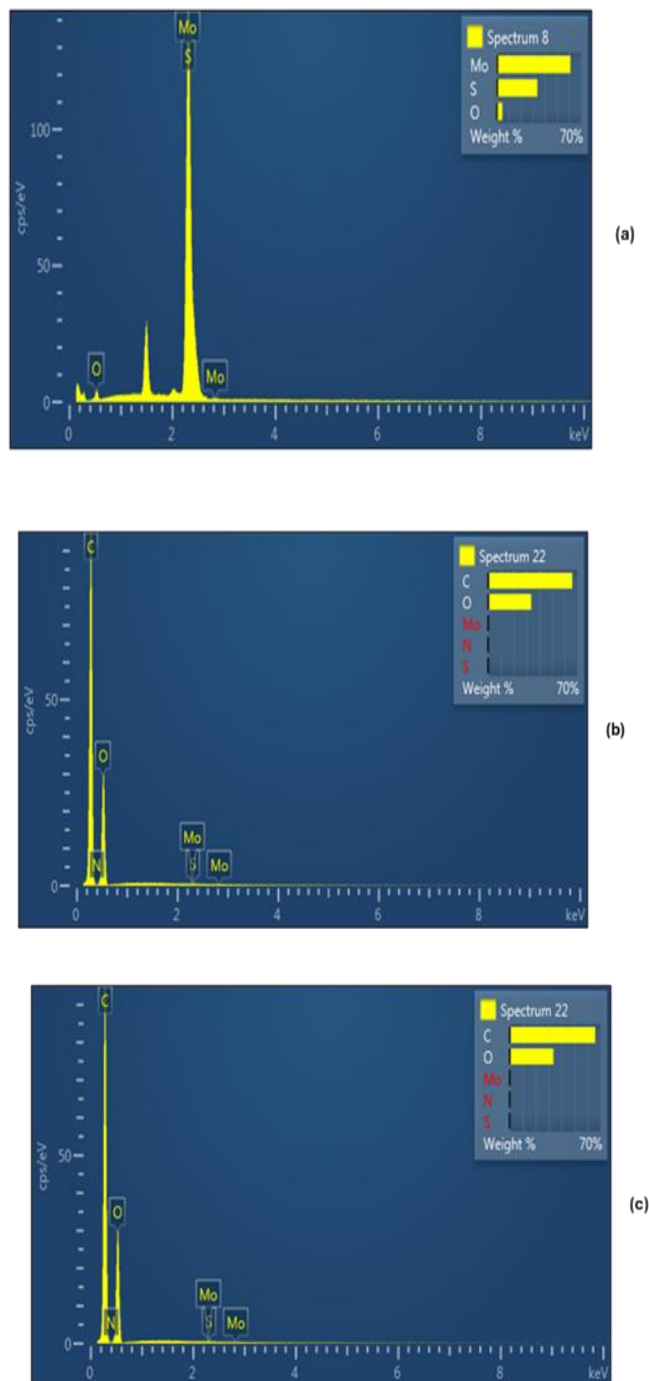


Figure 4. The EDX spectrum of (a) MoS₂, (b) MoS₂-CS, and (c) MoS₂-PEG

Figures 5a, b, and c show the XRD curves of pristine MoS₂, MoS₂-Chitosan (MoS₂-CS), and MoS₂-PEG composites, respectively. The main characteristic diffraction peaks of pure MoS₂ correspond to the hexagonal phase with the most conspicuous peaks at approximately 2 θ of 25° (004), 32.6° (100), 39.5° (103), 47° (105), and 58.3° (110), respectively, which are in good agreement with JCPDS file No. 37-1492. These peaks verify the successful synthesis of crystalline MoS₂ [38]. For the MoS₂-CS composite, the MoS₂ characteristic peaks are preserved, albeit with reduced peak intensity and slight broadening. The incorporation of chitosan alleviates the stacking and causes partial exfoliation of MoS₂ layers. Chitosan being a biopolymer, interacts with MoS₂ moieties via hydrogen bonding and/or electrostatic interactions which leads to a distortion in the regular packing of the MoS₂ nanosheets [38]. XRD pattern of MoS₂-PEG is sharper and more intense than MoS₂-CS. This means that PEG supports better stabilization and retains the crystallinity of MoS₂. PEG can interact with MoS₂ layers by physical adsorption or weak van der Waals forces, limiting the aggregation while still keeping the assembly of the material intact. The variations in intensity and sharpness of peaks for the three samples confirm the effect of polymer matrices on the structural properties of MoS₂. The lowered intensity and peak broadening for MoS₂-CS imply a loss of long-range order, while the sharper peaks for MoS₂-PEG demonstrate a more preserved crystal structure. Such structural changes agree well with the interaction mechanisms of the polymers with each other and the ensuing effects on the MoS₂ sheets.

Fourier-transform infrared (FTIR) spectroscopy is an important analytical instrument for the identification of chemical compounds in gases, liquids, powders, and films by the examination of their structural groups. It also enables the assessment of functional groups in polymeric materials by detecting stretching and bending vibration bands. Figure 6 shows the FTIR spectrum of the produced nanocomposite materials. The FTIR spectra of MoS₂

nanoparticles (Figure 6a) show distinctive peaks associated with Mo-S bonds. Significant absorption bands are seen at 687 cm⁻¹, 735 cm⁻¹, 1448 cm⁻¹, and 1624 cm⁻¹, corresponding to MoS₂. The peak at 466 cm⁻¹ is indicative of the S-S bond. The spectrum also displays characteristic peaks for Mo-O and Mo-S vibrations at around 587 cm⁻¹ and 470 cm⁻¹, respectively. The peak around 3426 cm⁻¹ corresponds to the distinctive O-H group bands [39]. Figure 6b displays the FTIR spectra of MoS₂-CS hybrid nanocomposites. The integration of Chitosan results in additional peaks associated with the functional groups present in chitosan. A pronounced peak at 3429 cm⁻¹ is ascribed to the O-H stretching vibration of hydroxyl groups. The peak at 1420 cm⁻¹ is attributed to the symmetrical deformation of CH₃, differentiating it from both virgin chitosan and MoS₂. The peak at 1154 cm⁻¹ is attributed to the C-O skeletal stretching vibration. In the FTIR spectra of MoS₂-CS composites, the -NH₂ signal at 1563 cm⁻¹ vanishes as a result of interactions with MoS₂ nanoparticles. Additionally, all peaks are displaced toward lower wavenumbers relative to clean chitosan [38]. The results indicate that polycationic chitosan engages with MoS₂ via nitrogen lone pairs, whereas the amine groups in chitosan draw MoS₂ through π - π stacking interactions [40]. Figure 6c illustrates the FTIR spectra of MoS₂-PEG hybrid nanocomposites, highlighting the presence of polyethylene glycol (PEG). A pronounced and strong band at 1109 cm⁻¹ corresponds to the C-O stretching mode, whilst a less intense nevertheless discernible band at 1465 cm⁻¹ is ascribed to the C-H bending mode vibration. A distinct band at 2883 cm⁻¹ signifies the weak stretching vibrational mode of C-H. These findings demonstrate that PEG functions as a coating for MoS₂ nanoparticles. Additionally, bands detected at 3457 cm⁻¹, 3741 cm⁻¹, and 3831 cm⁻¹ correspond to the stretching modes of inter- and intramolecular hydrogen bonds, together with hydroxyl groups absorbed from the environment [27]

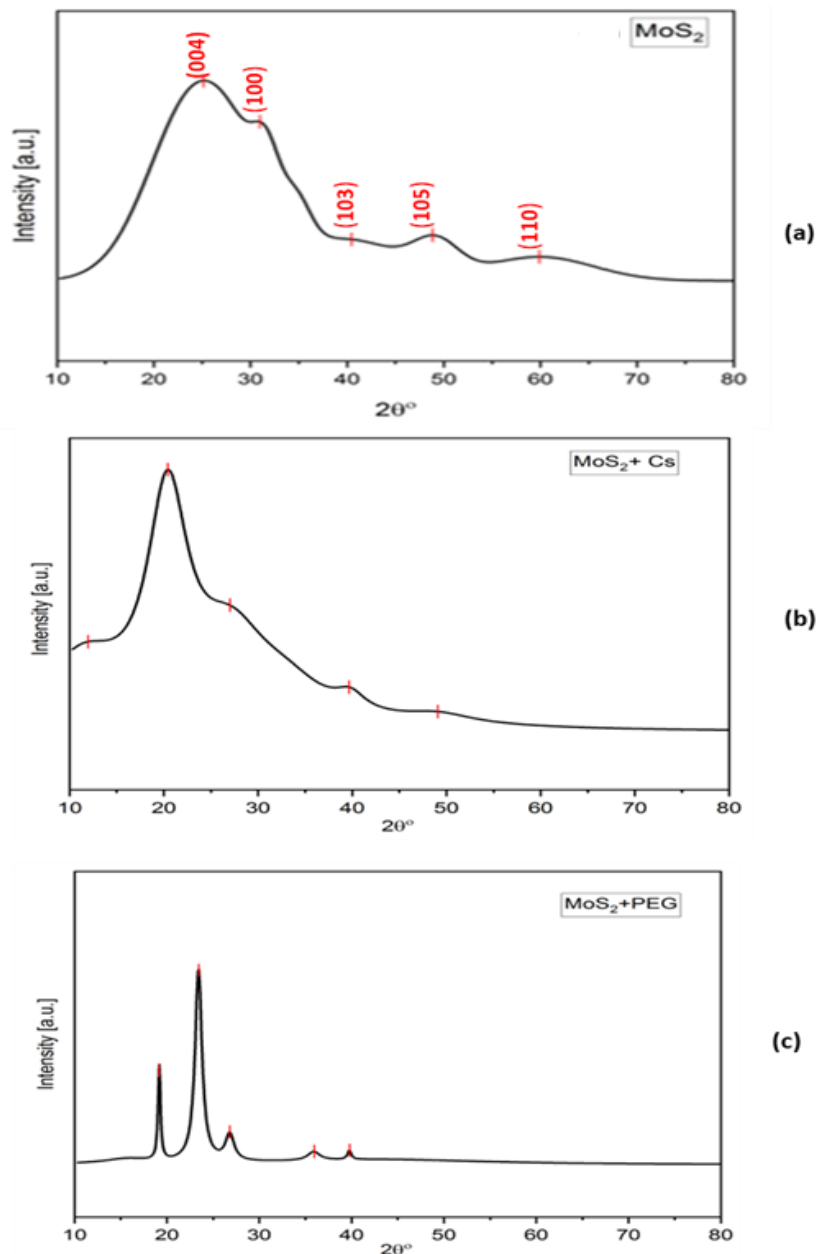


Figure 5. X-ray photoelectron spectra of (a) MoS₂, (b) MoS₂-CS, and (C) MoS₂-PEG

Raman spectroscopy was employed to analyze the atomic vibrations of MoS₂ nanoparticles and their nanocomposites. Figure 7a displays the Raman spectrum of bulk MoS₂, revealing two significant peaks corresponding to the in-plane (E_{2g}) mode at approximately 376 cm^{-1} and the out-of-plane (A_{1g}) mode at 448 cm^{-1} . The A_{1g} mode arises from the oscillation of sulfur atoms perpendicular to the basal plane, while the E_{2g} mode represents the in-plane vibrational

coupling of molybdenum and sulfur atoms in opposite directions [36]. The Raman spectrum of the MoS₂-CS nanocomposite is presented in Figure.7b. It exhibits the prominent E_{2g} and out-of-plane A_{1g} layered peaks at 398 cm^{-1} and 475 cm^{-1} , respectively. Notably, significant broadening of the Raman band peaks is observed compared to pristine MoS₂, indicating effective functionalization of chitosan onto the MoS₂ surfaces [41].

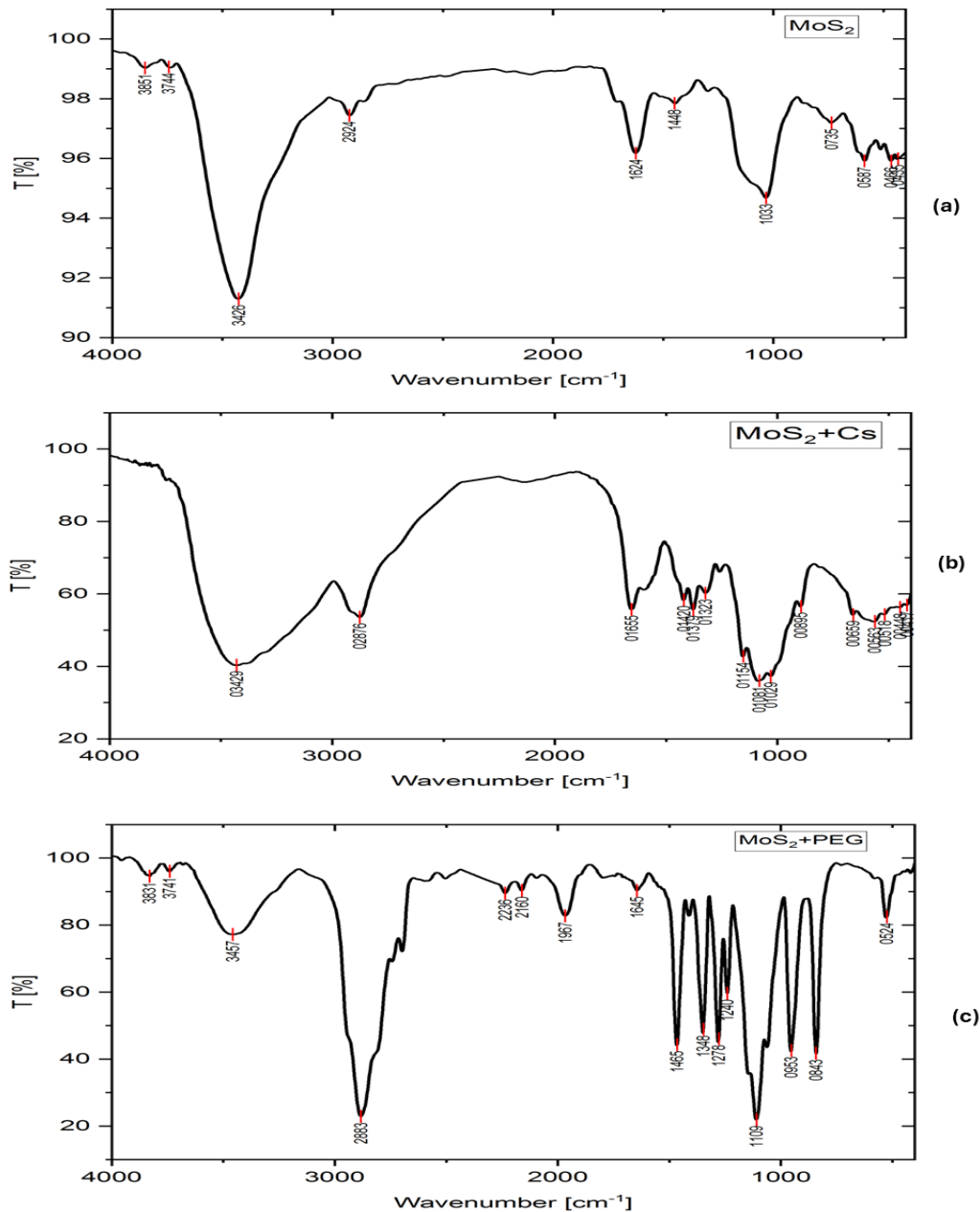


Figure 6. The FTIR of (a) MoS₂, (b) MoS₂-CS, and (c) MoS₂-PEG

Figure 7c illustrates the Raman spectrum of the MoS₂-PEG nanocomposite. In the low-frequency region (below 480 cm⁻¹), bands associated with the flexural vibrational modes of C–O and C–O–C bonds were identified, alongside low-to-medium vibrations of the PEG backbone. The band at 590 cm⁻¹ corresponds to

the C–C vibration within the PEG framework, accompanied by a prominent band at 1100 cm⁻¹. Additionally, the band at 992.7 cm⁻¹ is attributed to the stretching and bending modes of O–H bonds as well as the stretching of C–C bonds, characteristic of primary alcohols and prominently displayed in PEG [27].

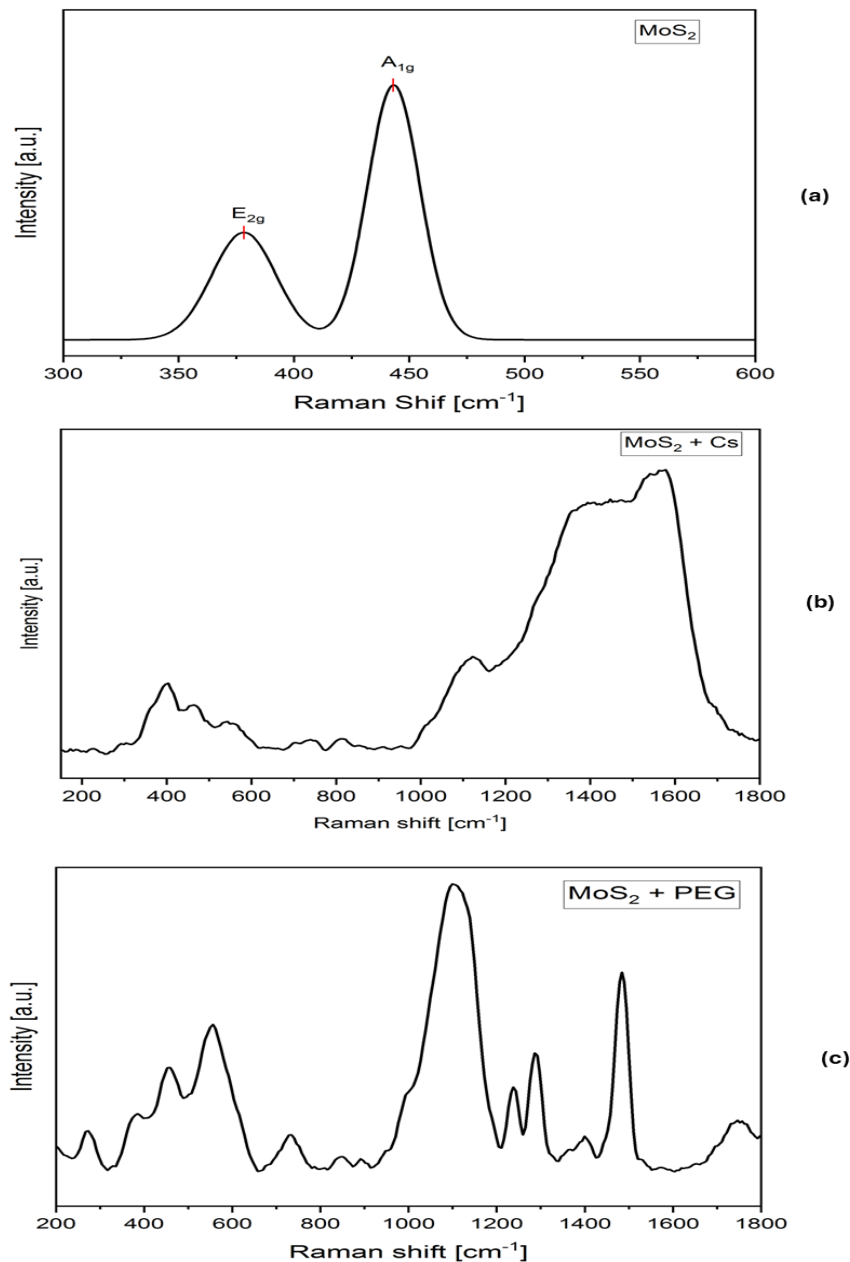


Figure 7. The Raman spectrum of (a) MoS₂, (b) MoS₂-CS, and (c) MoS₂-PEG

The antibacterial activity of laser-synthesized nanomaterials (MoS₂ NPs, MoS₂-PEG, and MoS₂-CS) and pure (CS and PEG) was carried out on two bacterial systems: *E. coli* (Gram-negative) and *S. aureus* (Gram-positive). These bacterial systems are predominantly found in soil, liquid, and gaseous environments. *Staphylococcus aureus* possesses a singular thick membrane layer composed of carbohydrates and amino acids, whereas *Escherichia coli* features many layers of proteins

and lipids, and it is the fundamental bacterial model for antibacterial tests.

The antibacterial activity and the obtained zone of inhibition results of nanocomposites against Gram-negative *E. coli* and Gram-positive *S. aureus* are shown in Figure 8 and Figure 9, respectively. The laser-synthesized nanomaterials had significant antibacterial activity against both bacterial strains. Figure 8 shows the obtained zone of inhibition results of MoS₂, MoS₂-PEG, MoS₂-CS, PEG, and CS against *E. coli* as 7.75, 9.6, 15.1, 6.1, and 7.1

mm, respectively (Table 2). Figure 9 shows the obtained zone of inhibition results of MoS₂, MoS₂-PEG, MoS₂-CS, PEG, and CS against *S. aureus* as 9.5, 17.25, 16.25, 6.1, and 9.5 mm, respectively (Table 2). The antibacterial activity of Figure 8 indicates that the MoS₂-CS nanocomposite was highly effective in inhibiting the growth of *E. coli* bacterial cells with 15.1 mm, and its antibacterial effect was significantly greater than pure MoS₂ and CS. Furthermore, the generated MoS₂-PEG nanocomposite recorded a 17.25 mm inhibition zone against *S. aureus* bacteria. The results show no antibacterial activity against both Gram-negative *E. coli* and Gram-positive *S. aureus* of pristine PEG, while its antibacterial activity is promoted by combining MoS₂ as MoS₂-CS, a nanocomposite. Pristine CS, on the other hand, shows antibacterial activity against both Gram-negative *E. coli* and Gram-positive *S. aureus*, which is further promoted by combining with MoS₂ as MoS₂-CS nanocomposite. The disparity in cell wall construction signifies the presence of variance in the inhibition rate. The results show that as the particle size decreased, as proved by TEM (Figure 3), the antibacterial performance gradually improved

by nanomaterial–bacteria contact-induced membrane stress by attaching contacting the membrane's surface and integrating into the membrane via creating indentations on the surface [42]. Indeed, the antibacterial effect is also attributed to the *E. coli* and *S. aureus* bacterial systems' absorption of the released metal cations (Mo⁺⁴) and nonmetal anions (S⁻²) from the nanocomposite materials. Cellular components are liberated from bacterial systems when absorbed cations adhere to the surface of the phospholipids in these systems[43]. The metal cations from MoS₂-CS and MoS₂-PEG are the true mediators of intracellular toxicity toward the tested bacterial systems. The antibacterial efficacy of these nanomaterials arises from the synergistic effects of membrane damage, oxidative stress, and metabolic inactivation.

The structural distinctions between Gram-positive and Gram-negative bacteria account for the disparities in susceptibility; Gram-positive bacteria possess simpler and thinner cell walls, rendering them more susceptible to antibacterial agents. Therefore, we notice that they are more affected by pure or composite nanomaterials, as shown in Table 2 [44].

Table 2: Antibacterial activity of pristine CS, PEG, MoS₂, MoS₂-CS, and MoS₂-PEG nanocomposites against *S. aureus* and *E. coli* bacteria obtained by the Agar diffusion method

Sample	Antibacterial analysis (Zone of inhibition (mm))					
	C	MoS ₂	MoS ₂ -PEG	MoS ₂ -CS	PEG	CS
<i>E. coli</i>	6.1	7.75	9.5	15.1	6.1	7.1
<i>S. aureus</i>	6.1	9.5	17.25	16.25	6.1	9.5

The particle size, concentration, morphology, shape, stability, specific surface area, technique, and treatment of the nanoparticles are critical elements affecting their antibacterial efficacy. The reduction in nanocomposite NP concentration is anticipated to increase H₂O₂ production, ultimately compromising bacterial cell membrane integrity, leading to cell leakage and death, as well as the creation and activity of ROS. The produced reactive oxygen species may harm several components inside bacterial

cells, such as the cell wall, mitochondria, plasma membrane, proteins, and DNA, while also disrupting electron transport, resulting in cell death[45].

Naturally, layered structured (2D) materials, such as molybdenum, and biopolymers like chitosan, are intriguing candidates for anticancer therapies due to their extensive surface area and stable, high oxidation states [43].

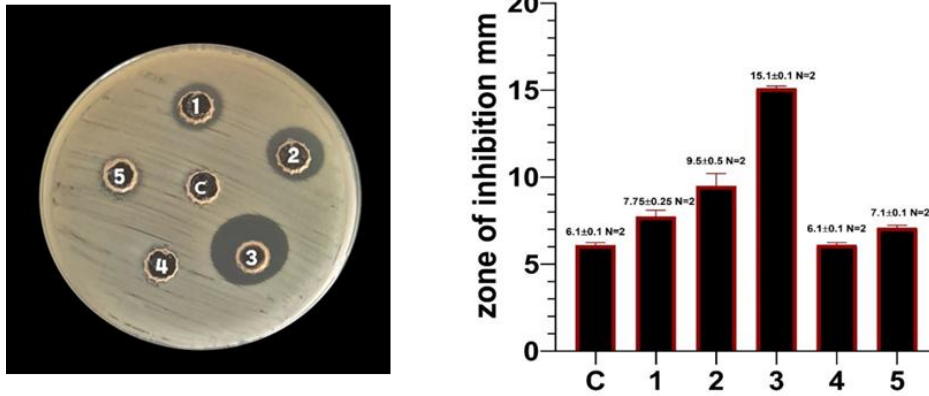


Figure 8. Antibacterial activity of nanomaterials against *E. coli*: C (Control), 1 (pure MoS₂), 2 (MoS₂-PEG), 3 (MoS₂-CS), 4 (PEG), and 5 (CS).

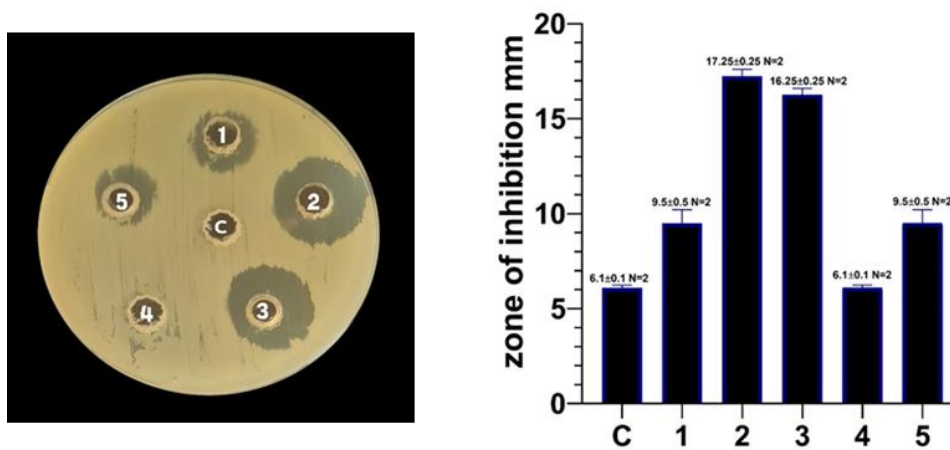


Figure 9. Antibacterial activity of nanomaterials against *S. aureus*: C (Control), 1 (pure MoS₂), 2 (MoS₂+PEG), 3 (MoS₂+CS), 4 (PEG) and 5 (CS)

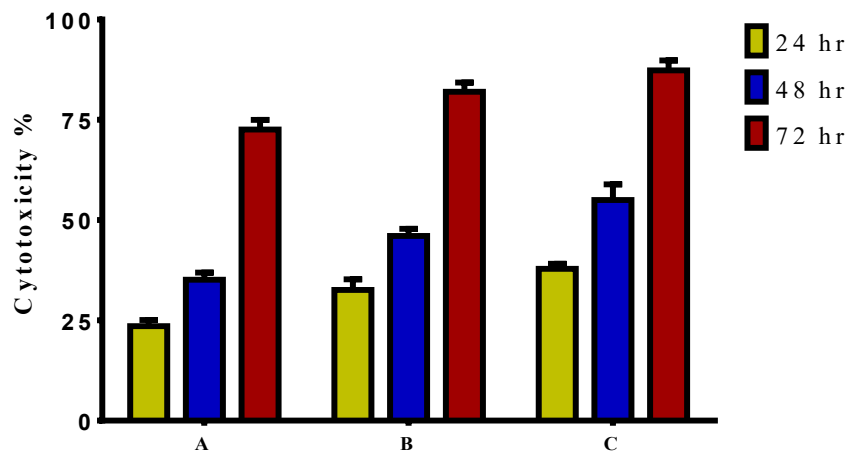
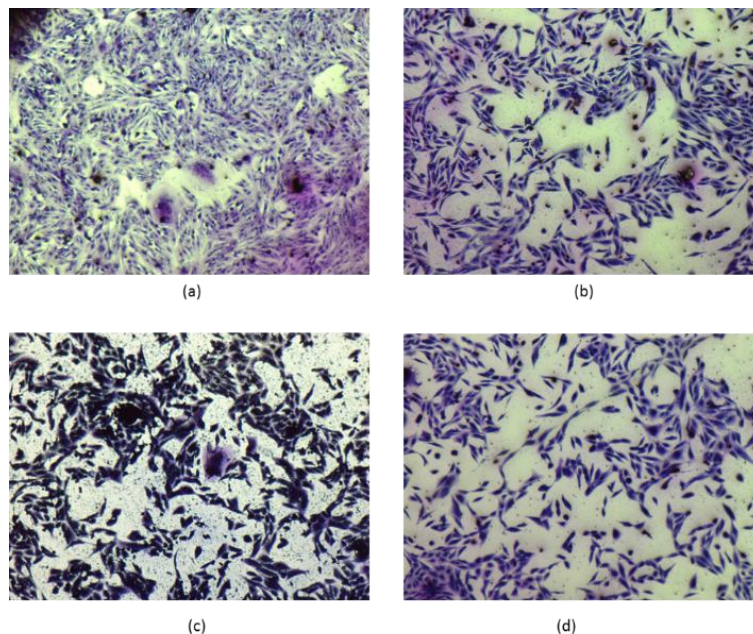
The cytotoxic effect of (NPs, NPs-PEG, and NPs-Chitosan) against A549 cells was studied (Figure 10). The antiproliferative activity of the (MoS₂, MoS₂-PEG, MoS₂-CS) was tested by studying their ability to inhibit cell proliferation (Figure 11).

From the anticancer results (Figure 10), MoS₂ shows 23.567%, 35.133%, and 72.567% of cell toxicity; MoS₂-PEG nanocomposite shows 32.567%, 46.033%, and 82% of cell inhibition; and MoS₂-CS nanocomposite shows 37.833%, 55%, and 87.333% of cell inhibition, corresponding to 24, 48 and 72 hrs. (Table 3 and

Figure 10). The results demonstrated that the MoS₂-CS nanocomposite has highly cytotoxic effects (Figure 10, Table 3) and all synthesized nanomaterials demonstrate a clear morphological change against the A549 cell line, as shown in Figure 11. The MoS₂-CS nanocomposite exhibits the highest cytotoxicity effect. The anticancer activity of MoS₂ nanocomposites due to the release of positive charge from polymer and Mo⁴⁺ ions, which generate reactive oxygen species (ROS) that induce the death of cancer cells[46].

Table 3: Anticancer activity of pristine MoS₂ and MoS₂-PEG, MoS₂-CS, nanocomposites against A549 cancer cell obtained by MTT assay method

Sample	Cytotoxicity %		
	24 hr	48 hr	72 h
MoS ₂	23.567	35.133	72.567
MoS ₂ -PEG	32.567	46.033	82
MoS ₂ -CS	37.833	55	87.333

**Figure 10.** Cytotoxicity effect of (MoS₂, MoS₂+PEG, MoS₂+CS) against A549 cells. (A) cells were treated with MoS₂, (B) Cells were treated with NPs-PEG, and (C) Cells were treated with NPs-Chitosan**Figure 11.** (a) Control untreated A549 cells, Morphological changes in A549 cells after being treated with (b) MoS₂ NPs, (c) MoS₂-PEG, and (d) MoS₂-CS. Magnification power 10x

3. Conclusions

In this study, MoS₂ nanoparticles (NPs) and MoS₂-CS, MoS₂-PEG hybrid nanocomposites were successfully synthesized via laser ablation and thoroughly characterized using various

analytical techniques. Results from X-ray diffraction (XRD), Raman spectroscopy, atomic force microscopy (AFM), and transmission electron microscopy (TEM) confirmed that the MoS₂ nanomaterials were well-dispersed,

highly compatible, and effectively anchored onto the chitosan and PEG matrices, forming a two-dimensional layered biopolymer structure. The XRD analysis revealed that the diffraction peaks of MoS₂ corresponded to a hexagonal crystalline structure. MoS₂ nanoparticles demonstrated significant absorption in the UV region, indicative of their optical properties. The MoS₂-CS nanocomposite exhibited notable antibacterial activity against (*E. coli*), while the MoS₂-PEG nanocomposite showed enhanced activity against (*S. aureus*) bacterial strains. Additionally, the MoS₂-CS hybrid nanocomposites displayed significant cell inhibition in anticancer evaluations. It can be concluded that the MoS₂-CS and MoS₂-PEG hybrid nanocomposites represent promising materials for biomedical applications, demonstrating both potent antibacterial and anticancer activities.

References

- [1] J. Lu *et al.*, "Molybdenum disulfide nanosheets: From exfoliation preparation to biosensing and cancer therapy applications," Oct. 01, 2020, *Elsevier B.V.* doi: 10.1016/j.colsurfb.2020.111162.
- [2] L. Ma *et al.*, "MoS₂ nanosheets vertically grown on carbonized corn stalks as lithium-ion battery anode," *ACS Appl Mater Interfaces*, vol. 10, no. 26, pp. 22067–22073, 2018.
- [3] L. Shi, L. Yang, Z. Wu, W. Xu, J. Song, and W. Guan, "Adenosine signaling: next checkpoint for gastric cancer immunotherapy?," *Int Immunopharmacol*, vol. 63, pp. 58–65, 2018.
- [4] X. Zhang and Y. Liang, "Nickel hydr (oxy) oxide nanoparticles on metallic MoS₂ nanosheets: a synergistic electrocatalyst for hydrogen evolution reaction," *Advanced Science*, vol. 5, no. 2, p. 1700644, 2018.
- [5] A. Zhang *et al.*, "An efficient and self-guided chemo-photothermal drug loading system based on copolymer and transferrin decorated MoS₂ nanodots for dually controlled drug release," *Chemical Engineering Journal*, vol. 342, pp. 120–132, 2018.
- [6] H. Liu *et al.*, "MoS₂ nanosheets with peroxidase mimicking activity as viable dual-mode optical probes for determination and imaging of intracellular hydrogen peroxide," *Microchimica Acta*, vol. 185, pp. 1–9, 2018.
- [7] M. Karami and O. M. Jazani, "The Progress of Molybdenum Disulfide 2D Nanosheets as Bionanocarriers for Drug Delivery Systems: A Groundbreaking Approach with Multiple Therapeutic Applications," *J Inorg Organomet Polym Mater*, pp. 1–30, 2025.
- [8] A. M. Allahverdiyev, K. V. Kon, E. S. Abamor, M. Bagirova, and M. Rafailovich, "Coping with antibiotic resistance: combining nanoparticles with antibiotics and other antimicrobial agents," *Expert Rev Anti Infect Ther*, vol. 9, no. 11, pp. 1035–1052, 2011.
- [9] M. Kukkar, S. K. Tuteja, P. Kumar, K.-H. Kim, A. S. Bhadwal, and A. Deep, "A novel approach for amine derivatization of MoS₂ nanosheets and their application toward label-free immunosensor," *Anal Biochem*, vol. 555, pp. 1–8, 2018.
- [10] B. J. Carey *et al.*, "Two solvent grinding sonication method for the synthesis of two-dimensional tungsten disulphide flakes," *Chemical Communications*, vol. 51, no. 18, pp. 3770–3773, 2015.
- [11] G. Cunningham *et al.*, "Solvent exfoliation of transition metal dichalcogenides: dispersibility of exfoliated nanosheets varies only weakly between compounds," *ACS Nano*, vol. 6, no. 4, pp. 3468–3480, 2012.
- [12] R. J. Smith *et al.*, "Large-scale exfoliation of inorganic layered compounds in aqueous surfactant solutions," *Advanced materials*, vol. 23, no. 34, pp. 3944–3948, 2011.
- [13] J. N. Coleman *et al.*, "Two-dimensional nanosheets produced by liquid exfoliation of layered materials," *Science (1979)*, vol. 331, no. 6017, pp. 568–571, 2011.
- [14] L. Muscuso, S. Cravanzola, F. Cesano, D. Scarano, and A. Zecchina, "Optical, vibrational, and structural properties of MoS₂ nanoparticles obtained by exfoliation and fragmentation via ultrasound cavitation in isopropyl alcohol," *The Journal of Physical Chemistry C*, vol. 119, no. 7, pp. 3791–3801, 2015.
- [15] G. Pagona, C. Bittencourt, R. Arenal, and N. Tagmatarchis, "Exfoliated semiconducting pure 2H-MoS₂ and 2H-WS₂ assisted by chlorosulfonic acid," *Chemical Communications*, vol. 51, no. 65, pp. 12950–12953, 2015.
- [16] A. O'Neill, U. Khan, and J. N. Coleman, "Preparation of high concentration dispersions of exfoliated MoS₂ with increased flake size," *Chemistry of Materials*, vol. 24, no. 12, pp. 2414–2421, 2012.
- [17] K. S. Khashan, A. A. Hadi, and I. F. Hasan, "Nanosecond Laser-Supported Decoration of Titanium Oxide Nanoparticles on Multiwalled Carbon Nanotubes," *Plasmonics*, vol. 19, no. 1, pp. 301–310, 2024.
- [18] K. S. Khashan, B. A. Badr, G. M. Sulaiman, M. S. Jabir, and S. A. Hussain, "Antibacterial activity of Zinc Oxide nanostructured materials synthesis by laser ablation method," in *Journal of physics: conference series*, IOP Publishing, 2021, p. 012040.
- [19] N. Acacia, F. Barreca, E. Barletta, D. Spadaro, G. Currò, and F. Neri, "Laser ablation synthesis of indium oxide nanoparticles in water," *Appl Surf Sci*, vol. 256, no. 22, pp. 6918–6922, 2010.

- [20] L. Zhou, H. Zhang, H. Bao, G. Liu, Y. Li, and W. Cai, "Onion-Structured Spherical MoS₂ Nanoparticles Induced by Laser Ablation in Water and Liquid Droplets' Radial Solidification/Oriented Growth Mechanism," *Journal of Physical Chemistry C*, vol. 121, no. 41, pp. 23233–23239, Oct. 2017, doi: 10.1021/acs.jpcc.7b07784.
- [21] M. Kanazawa, P. Koinkar, K. I. Murai, T. Moriga, and A. Furube, "Effects of the solvent during the preparation of MoS₂ nanoparticles by laser ablation," in *Journal of Physics: Conference Series*, Institute of Physics Publishing, Sep. 2019. doi: 10.1088/1742-6596/1230/1/012100.
- [22] S. Moniri, A. H. Mohammad Zadeh, A. H. Ramezani, and M. R. Hantehzadeh, "Influence of laser wavelength on the optical and structural properties of MoS₂ nanoparticles prepared via laser irradiation in ethylene glycol," *J Laser Appl*, vol. 33, no. 3, p. 032013, Jul. 2021, doi: 10.2351/7.0000361.
- [23] S. Moniri and M. R. Hantehzadeh, "Colloidal synthesis of MoS₂ NPs by nanosecond laser ablation of a bulk MoS₂ target in ethylene glycol solution," *Opt Quantum Electron*, vol. 53, no. 5, May 2021, doi: 10.1007/s11082-021-02872-5.
- [24] F. Ye *et al.*, "Synthesis of Two-Dimensional Plasmonic Molybdenum Oxide Nanomaterials by Femtosecond Laser Irradiation," *Chemistry of Materials*, vol. 33, no. 12, pp. 4510–4521, Jun. 2021, doi: 10.1021/acs.chemmater.1c00732.
- [25] P. Zuo *et al.*, "MoS₂ core-shell nanoparticles prepared through liquid-phase ablation and light exfoliation of femtosecond laser for chemical sensing," *Sci China Technol Sci*, vol. 66, no. 3, pp. 853–862, Mar. 2023, doi: 10.1007/s11431-022-2270-9.
- [26] Z. Wang *et al.*, "Fabrication of micro/nano wettability MoS₂ hydrogen evolution electrocatalyst based on femtosecond laser," *Int J Hydrogen Energy*, vol. 51, pp. 327–335, Jan. 2024, doi: 10.1016/j.ijhydene.2023.08.160.
- [27] T. R. S. Malagrino *et al.*, "Multifunctional Hybrid MoS₂-PEGylated/Au Nanostructures with Potential Theranostic Applications in Biomedicine," *Nanomaterials*, vol. 12, no. 12, Jun. 2022, doi: 10.3390/nano12122053.
- [28] M. H. Karami and M. Abdouss, "Advancements in utilizing exosomes for cancer therapy through drug delivery systems: recent developments.," *Nanomed J*, vol. 12, no. 2, 2025.
- [29] M. Karami, M. Pourmadadi, M. Abdouss, and M. Kalaei, "Synthesis, Characterization, and In Vitro Analysis of a Chitosan/Gamma Alumina/Graphene Quantum Dots/Bio-Hydrogel for Quercetin Delivery to Lung Cancer Cells," *Bionanoscience*, vol. 15, no. 1, pp. 1–19, 2025.
- [30] W. Zhang *et al.*, "Versatile molybdenum disulfide based antibacterial composites for in vitro enhanced sterilization and in vivo focal infection therapy," *Nanoscale*, vol. 8, no. 22, pp. 11642–11648, 2016.
- [31] T. Liu *et al.*, "Drug delivery with PEGylated MoS₂ nano-sheets for combined photothermal and chemotherapy of cancer.," *Adv Mater*, vol. 26, no. 21, pp. 3433–3440, 2014.
- [32] W. A. Salih, "SYNTHESIS AND CHARACTERIZATION OF LASER-ABLATED SILVER AND TITANIUM OXIDE NANOPARTICLES: IMPLICATIONS FOR DRUG DELIVERY," *New Materials, Compounds and Applications*, vol. 8, no. 2, pp. 199–222, Aug. 2024, doi: 10.62476/nmca82199.
- [33] M. S. Jabir *et al.*, "Inhibition of Staphylococcus aureus α -hemolysin production using nanocurcumin capped Au@ ZnO nanocomposite," *Bioinorg Chem Appl*, vol. 2022, no. 1, p. 2663812, 2022.
- [34] S. Al-Musawi, S. Albukhaty, H. Al-Karagoly, G. M. Sulaiman, M. S. Jabir, and H. Naderi-Manesh, "Dextran-coated superparamagnetic nanoparticles modified with folate for targeted drug delivery of camptothecin," *Advances in Natural Sciences: Nanoscience and Nanotechnology*, vol. 11, no. 4, p. 045009, 2020.
- [35] M. S. Jabir *et al.*, "Gold nanoparticles loaded TNF- α and CALNN peptide as a drug delivery system and promising therapeutic agent for breast cancer cells," *Materials Technology*, vol. 37, no. 14, pp. 3152–3166, 2022.
- [36] K. C. Lalithambika, K. Shanmugapriya, and S. Sriram, "Photocatalytic activity of MoS₂ nanoparticles: an experimental and DFT analysis," *Appl Phys A Mater Sci Process*, vol. 125, no. 12, Dec. 2019, doi: 10.1007/s00339-019-3120-9.
- [37] X. Huang, C. Tan, Z. Yin, and H. Zhang, "25th anniversary article: Hybrid nanostructures based on two-dimensional nanomaterials," Apr. 09, 2014, Wiley-VCH Verlag. doi: 10.1002/adma.201304964.
- [38] K. Kasinathan, B. Murugesan, N. Pandian, S. Mahalingam, B. Selvaraj, and K. Marimuthu, "Synthesis of biogenic chitosan-functionalized 2D layered MoS₂ hybrid nanocomposite and its performance in pharmaceutical applications: In-vitro antibacterial and anticancer activity," *Int J Biol Macromol*, vol. 149, pp. 1019–1033, Apr. 2020, doi: 10.1016/j.ijbiomac.2020.02.003.
- [39] K. C. Lalithambika, K. Shanmugapriya, and S. Sriram, "Photocatalytic activity of MoS₂ nanoparticles: an experimental and DFT analysis," *Applied Physics A*, vol. 125, pp. 1–8, 2019.
- [40] L. Ma, X. Zhou, L. Xu, X. Xu, L. Zhang, and W. Chen, "Chitosan-assisted fabrication of ultrathin MoS₂/graphene heterostructures for Li-ion battery with excellent electrochemical performance," *Electrochim Acta*, vol. 167, pp. 39–47, 2015.
- [41] W. Yin *et al.*, "High-throughput synthesis of single-layer MoS₂ nanosheets as a near-infrared photothermal-triggered drug delivery for effective cancer therapy," *ACS Nano*, vol. 8, no. 7, pp. 6922–6933, 2014.
- [42] T. Cheng *et al.*, "A spray-freezing approach to reduced graphene oxide/MoS₂ hybrids for superior

- energy storage,” *Energy Storage Mater*, vol. 10, pp. 282–290, 2018.
- [43] L.-Q. Fan, G.-J. Liu, C.-Y. Zhang, J.-H. Wu, and Y.-L. Wei, “Facile one-step hydrothermal preparation of molybdenum disulfide/carbon composite for use in supercapacitor,” *Int J Hydrogen Energy*, vol. 40, no. 32, pp. 10150–10157, 2015.
- [44] T. J. Silhavy, D. Kahne, and S. Walker, “The bacterial cell envelope,” *Cold Spring Harb Perspect Biol*, vol. 2, no. 5, p. a000414, 2010.
- [45] M. H. Heng *et al.*, “Microwave-assisted green synthesis, characterization, and in vitro antibacterial activity of NiO nanoparticles obtained from lemon peel extract,” *Green Processing and Synthesis*, vol. 13, no. 1, p. 20240071, 2024.
- [46] X. Lu *et al.*, “One-step hydrothermal fabrication of three-dimensional MoS₂ nanoflower using polypyrrole as template for efficient hydrogen evolution reaction,” *Sci Rep*, vol. 7, no. 1, p. 42309, 2017.